Uncertainty Assessment of Dynamic Thermal Line Rating for Operational Use at Transmission System Operators

Aleksandra Rashkovska, *Member, IEEE,* Mitja Jančič, Matjaž Depolli, Janko Kosmač, and Gregor Kosec, *Member, IEEE*

Abstract—Transmission system operators (TSOs) in recent years have faced challenges in order to ensure maximum transmission capacity of the system to satisfy market needs, while maintaining operational safety and permissible impact on the environment. A great help in the decision-making process was introduced with the Dynamic Thermal Rating (DTR) – an instrument to monitor and predict the maximal allowed ampacity of the power grid based on weather measurements and forecast. However, the introduction of DTR raises a number of questions related to the accuracy and uncertainty of the results of thermal assessment and the level of acceptable risk and its management. In this paper, we present a solution for estimating DTR uncertainty, appropriate for operational use at TSOs. With the help of conductor surface temperature measurements, weather measurements and predicted weather data, we also estimate the error of the weather forecast and the DTR itself. Following the results of the data analyses, we build an operative solution for estimating the ampacity uncertainty based on Monte Carlo random simulations and integrate it into the operational environment of ELES – the operator of the Slovenian electric power transmission network.

Index Terms—Dynamic Thermal Rating, Transmission line, Transmission System Operator, Ampacity, Uncertainty, Forecast, Probability Distribution Function, Monte Carlo.

I. INTRODUCTION

IN the last years, we have witnessed an extremely rapid development of the electricity market and services, mainly due to the inclusion of renewable energy resources in the network, which can cause extensive and rapid changes in the electrical power load. Combined with growing power consumption, the existing power transmission lines are utilized to much higher extent than they were in the past. This has already led to critical bottlenecks and, in the worst scenarios, also to system-wide instabilities, resulting in blackouts, e.g. the disturbance in 2006 [1], or the Italian blackout in 2003 [2].

The occurrence of instabilities in the power grid encouraged the transmission system operators (TSOs) to re-evaluate the

measures for maintaining system stability and to find a way to better utilize the existing infrastructure. A great help in this process was introduced with the Dynamic Thermal Rating (DTR) [3] – an instrument for predicting the temperature of a transmission line based on the load and weather conditions, measured or predicted. The temperature of a transmission line is often a limiting factor of the power transmission capacity. However, instead in conductor temperature, TSOs are often interested in ampacity – the maximal allowed current before the power line reaches critical temperature, which is fully determined by the weather data and the material properties of the power line.

TSOs, for the most part, use DTR to alleviate the infrastructural deficiencies that emerge due to the extensive financial burden and vast societal consensus for environmental care when acquiring new transmission corridors. Reliable DTR is also an important part in congestion management of power systems [4], especially in operation and planning of power systems where renewable energy intermittencies exist [5, 6]. DTR models have been gradually improved in the last few decades by including more and more refined physical models for various phenomena, ranging from rain impinging to different parametrisation of convective cooling [7]–[10]. The advancements in the DTR research community are periodically collected and presented in comprehensive DTR guidelines provided by the CIGRE [3], IEEE [11] and IEC [12] standards. The evolution of DTR physical models and methods, and their integration into operational use, are thoroughly discussed in recent review papers [13, 14].

The introduction of DTR raised a number of questions related to the uncertainty of the computed ampacity, level of acceptable risk and its management. Traditionally, TSOs allow power lines to be utilized up to a static thermal limit, which is calculated based on relatively conservative weather parameters (high temperature and sun radiation, and low wind), and provides safe and secure operation of the power line. With the advent of DTR systems, which use an indirect approach to the calculation of the dynamic thermal value, i.e. use of weather parameters along the power line, the question on how accurate is the dynamic line rating popped-up. Therefore, in the last years, a growing interest has been shown in applying probabilistic methods to weather-based DTR procedures, in order to account for the uncertainty of forecasting ambient conditions. Although recently several machine learning approaches have been also applied for probabilistic DTR forecasting [15]–[17],

the Monte Carlo method is still the most widely used approach to draw possible deviations in DTR with respect to weather forecasts [18]–[20].

By using probabilistic approaches, the ampacity of a line is described, instead by a scalar value as in the standard DTR approach, with a Probability Distribution Function (PDF). By means of Monte Carlo (MC) simulations [21], the uncertainty of the input parameters to the DTR model, i.e. the weather forecast uncertainty, is transformed into uncertainty of the predicted ampacity. This approach was proposed for the first time in [22] and then further developed by other researchers [18, 19, 23, 24]. Nevertheless, in these papers, the meteorological data was assumed to follow *a priori* Gaussian distribution, which is a strong assumption not supported by real data observations. In a recent paper [20], the authors propose that the PDFs of weather parameters, which are employed to feed the thermal model of the line in order to assess its uncertainty, are tuned to the actual weather forecasting errors at a certain location.

In this paper, we also use the weather data measurements and the weather forecast data in the proximity of a transmission line, and combine them with the conductor surface temperature measurements, to determine the expected uncertainty of DTR prediction. What separates our study, compared to previous related work, is that we present a concrete solution procedure on how to put a DTR uncertainty assessment module in operation, calibrated for a specific location, i.e. operating point. The presented solution procedure could be useful for any TSO. Moreover, compared to previous studies, we examine the dependence of the ampacity distribution not only on the weather conditions (air temperature, solar irradiance, and wind speed and direction), but also on the conductor type and emissivity. We also assess the weather uncertainty, examining the dependence of the forecast error on the forecast horizon. Finally, we assess the DTR uncertainty introduced by the the DTR model itself.

The rest of the paper is organized as follows. In Section II, we present and analyse the weather data provided by the TSO. Section III describes the proposed solution procedure for the assessment of the DTR uncertainty using MC simulations. Before presenting the implementation of the proposed solution for operational use at TSOs in Section V, some prior analyses, aimed at simplifying the implementation, are made in Section IV. The paper finalizes with the conclusions presented in Section VI.

II. WEATHER DATA

As it will be demonstrated in Section III, the main source of ampacity prediction uncertainty stems from uncertainty of weather data. Therefore, to understand the uncertainty of ampacity prediction, we have to first analyse the uncertainty of weather data, which is the goal in this section.

The data for the study has been provided by the Slovenian TSO ELES for two locations in Slovenia: Podlog (Obersielach-Podlog transmission line) and Bevkov vrh (Cerkno-Idrija transmission line). The weather data was measured with two weather stations at the mentioned locations with a time resolution of 5 minutes. The time span covers almost all of year

2019 and a part of year 2020. From the data, we have extracted the following measured weather parameters:

- T [°C]: ambient temperature,
- S [W/m^2]: solar irradiance,
- v [m/s]: wind speed,
- ϕ [°]: wind direction referencing the north.

In the following, these data will be referred to as *measured* weather data. On the other hand, *predicted* weather data will refer to the data coming from the weather forecast model of the TSO, which is derivative of the Aladin model provided by the Slovenian Environment Agency. The predicted weather data is consisted of two sets:

- Assessment of current weather conditions or *nowcast*.
- Predicted weather data for different time horizons, in the range between 0 and 72 hours in the future.

Such a data structure allows the relationship between the error distributions for the weather parameters and the time horizon of the weather forecast to be investigated.

The goal here is to prepare the input data for the MC simulations, i.e., the error distributions of the weather parameters computed as the difference between the measured and the predicted values. We start with the analysis of the error distributions for the nowcast, given in Fig. 1. For the error distribution of the solar irradiance, we can observe a large spike at the value of zero. Such a spike is expected since these examples belong to the solar irradiance during the night, which is close to zero and is predominantly correctly predicted. Therefore, we omit the examples where the predicted solar irradiance is zero and recalculate the error distribution for the solar irradiance. The resulting PDF is given in Fig. 2. In the following, we refer to this distribution as the solar error distribution.

At a first glance, the error distributions for all weather parameters do not seem to belong to a normal Gaussian distribution, as usually assumed in the literature [18, 19, 23, 24]. We have tested this hypothesis using the Kolmogorov-Smirnov normality test. The test rejected the hypothesis for all weather parameters with a high significance level (p value < 0.0001). This is also visually demonstrated by fitting normal distribution (red curve) over the error distributions shown in Fig. 1 and Fig. 2. Therefore, the goal would be to fit the error data to a custom kernel distribution for each variable separately.

Next, we look into the dependence of the weather forecast error on the forecast horizon. The question asked here is: "*How does the weather forecast error increase with time?*". We compare the error distributions of the weather nowcast and forecast for different time horizons for each of the weather parameters. Two error distributions for the weather forecast for different time horizons are analysed:

- error distribution for the weather forecast for the time horizon 0-12 hours, referred to as *short-term* forecast, and
- error distribution for the weather forecast for the time horizon 12-72 hours, referred to as *medium-term* forecast.

Fig. 3 shows the error distribution of the nowcast, and for the short- and medium-term forecasts, for each weather
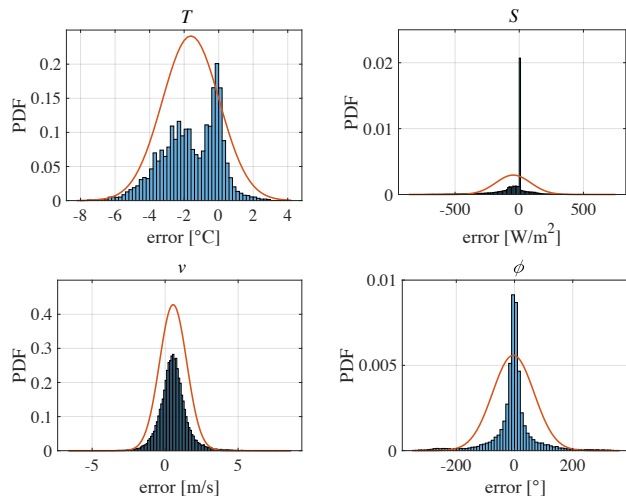
Fig. 1. Error distribution for the weather parameters, compared to normal distribution (red curve), for Bevkov vrh.

Fig. 3. Error distributions for the weather parameters for different forecast horizons for Bevkov vrh.
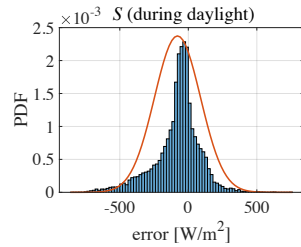

Fig. 2. Error distribution for the solar irradiance, omitting the zero values, compared to normal distribution (red curve), for Bevkov vrh.

parameter for Bevkov vrh. We can observe that, as expected, the nowcast is significantly more accurate than the forecast, while the difference between the short- and medium-term forecasts are not that expressive. For each weather parameter, a two-sample Kolmogorov-Smirnov test was used to test the hypotheses that each pair of error data for different time horizons come from the same distribution. The tests rejected all hypotheses, except the ones for wind speed and direction for the comparison between short- and medium-term forecast distributions. Effectively, this means that the weather forecast spread is wide enough at a given forecast time span, so different error distributions should be used for different forecast horizons.

III. CONCEPT OF THE AMPACITY UNCERTAINTY ASSESSMENT

In this section, we describe the procedure for obtaining the uncertainty of the DTR. The core of the solution procedure are MC simulations. The first step in solving uncertainty problems with the MC method is to build or provide the model between the output and the inputs, which, in our case is DTR model – a physical model that transforms the input weather parameters to the output ampacity, i.e. the maximal load at which the power line temperature will not exceed a predefined critical temperature. In this study, we use the extended CIGRE [3] DTR model – DiTeR [7], which is in operative use at the Slovenian TSO ELES since 2019. The
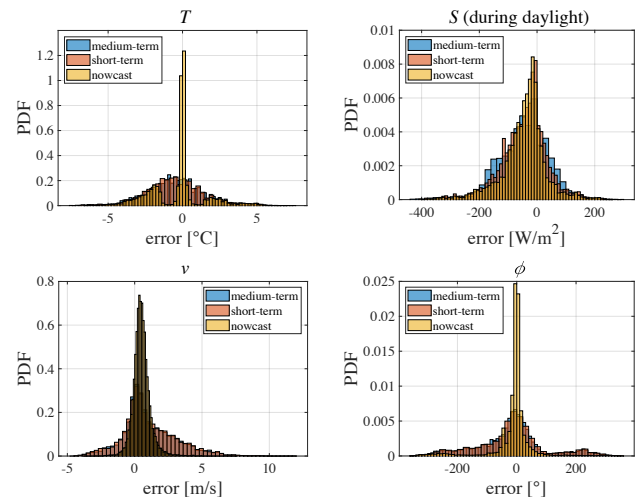
physical model comprises Joule heating, convective cooling, solar heating, cooling due to evaporation, and radiation. In its essence, the model solves the heat transport equation (second-order partial differential equation) with non-linear boundary conditions, describing different heat terms due to the weather conditions [7]. By solving the heat transport, DiTeR computes the temperature profile within the conductor, assuming the line load is known, or the ampacity.

The next step in the uncertainty assessment with the MC method is the preparation of the input probability distributions, i.e. the PDFs of the weather parameters. Once the PDFs for all input parameters are known, the MC procedure samples them by the inverse transformation methods and transforms the input PDFs to the output PDF, namely the distribution of ampacity. If we suppose that the confidence interval corresponding to the output confidence of $100p\%$ is required, where p is the value of confidence level, then the number of MC repeated calculations is M times, where M satisfies $M \geq \frac{1}{10p}10^4$ [24].

The solution procedure is shown schematically in Fig. 4. It starts by using the measured data to determine the errors of the input variables. To obtain a PDF from the samples of weather forecasting errors, a kernel distribution is fitted over the error data for each variable separately using the Epanechnikov kernel that optimizes the mean square error between the data and the fit. In the next step, the weather forecast error distributions are offset to the given weather conditions T_0, S_0, v_0 and ϕ_0, which gives us the spread of the given weather conditions, namely the PDFs for temperature $\mathcal{T}(T)$, solar irradiance $\mathcal{S}(S)$, wind speed $\mathcal{V}(v)$ and wind direction $\Phi(\phi)$. The constructed PDFs are truncated at unrealistic values, namely negative wind speed, and negative solar irradiance or solar irradiance above the solar constant. Then, using the MC method, the PDFs prepared in the previous step are transformed into ampacity distribution $\mathcal{I}_{th}$ normalized with the *nominal ampacity* I_{th_0}, i.e. the ampacity computed with DTR at T_0, S_0, v_0 and ϕ_0. Finally, the lower I_{th}^{lo} and upper I_{th}^{hi} limits of ampacity are computed by integrating $\mathcal{I}_{th}$ from the Cumulative Distribution Function (CDF) using cumulative
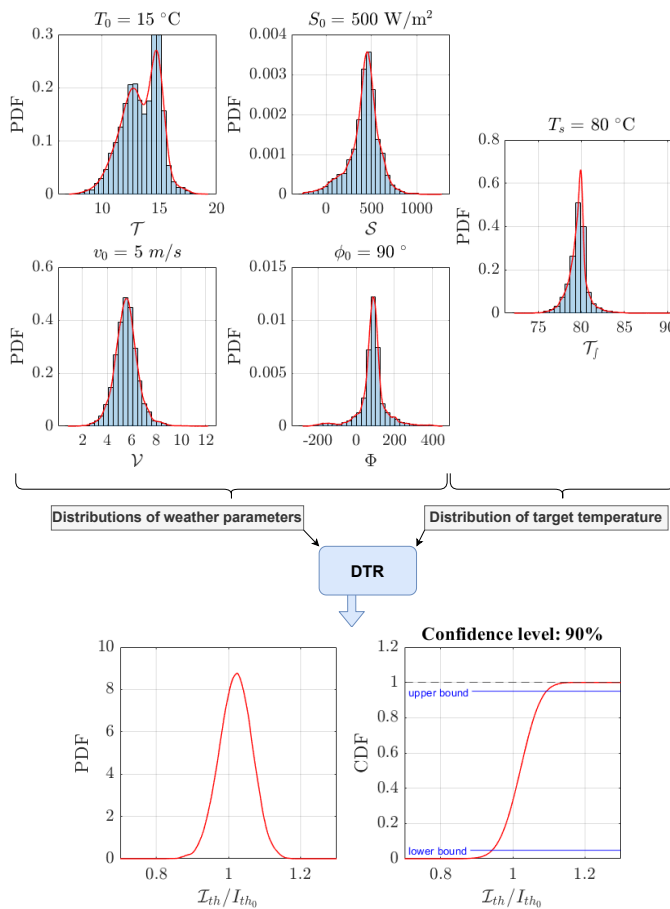
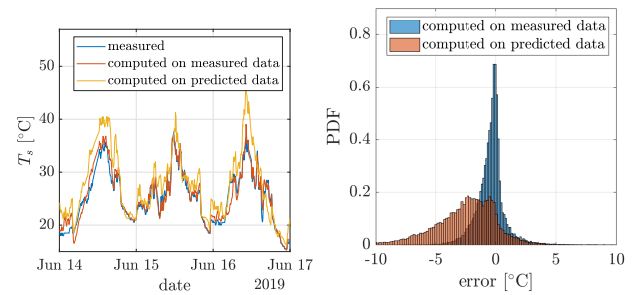Fig. 4. Conceptual representation of the DTR uncertainty estimation.

Fig. 5. Time evolution of conductor temperature: measured, computed with measured weather data and computed with weather forecast data (left). Error distribution of conductor temperature computed with measured and forecasted weather parameters (right).

trapezoidal numerical integration, and then searching for the values of I_{th} for which CDF(I_{th}) equals $\frac{p}{2}$ and $1 - \frac{p}{2}$, respectively.

The uncertainty of DTR stems not only from the uncertainty of the weather forecast but also from the error of the DTR model itself. The latter can be assessed using conductor skin temperature (T_s) measurements provided from the TSO for the transmission lines on both investigated locations. In Fig. 5 (left), the measured skin temperature of the conductor is compared to the modelled temperature computed using the measured instead of modelled meteorological weather data. This way, the generated error includes only the error of the DTR model and the measurement error of the used sensors, but it no longer includes the error of the weather nowcast/forecast. In addition to the DTR calculation based on the measured weather data, we also compute the conductor temperature with the nowcast meteorological data. Introducing the DTR error as a difference between computed and measured conductor skin temperature, we can prepare DTR error distributions (Fig. 5 (right)). We can see that the error induced by the weather uncertainty dominates, even for the nowcast.

IV. IMPACT OF WEATHER UNCERTAINTY AND CONDUCTOR PROPERTIES ON AMPACITY UNCERTAINTY

In operational use, the ampacity for all spans in the power grid is typically computed every time new data becomes available. In the case of the Slovenian network, this happens every minute. Using MC for uncertainty assessment for each ampacity prediction would result in a large computational burden. Therefore, before implementing the proposed procedure in operational use by the TSO, some prior analyses have been made to optimize the actual implementation by understanding the relationships between the uncertainty of ambient factors, material properties and the uncertainty of the ampacity. Foremost, prior analyses have been made to identify which weather parameters and material properties of the conductor influence the ampacity probability distribution the most.

First, we examine the impact of the weather parameters on the ampacity uncertainty. According to our preliminary analysis of weather parameters, we calculate normalized ampacity PDFs for each combination (sub-space) of wind speed $v \in \{0.15; 0.5; 2; 5; 15\}$ m/s and wind direction $\phi \in \{0, 45, 90\}°$, for the conductor type 243-AL1/39 and emissivity of 0.9. Furthermore, for each wind speed and angle combination, 9 more combinations for ambient temperature $T \in \{0, 15, 30\}$ °C and solar irradiance $S \in \{100, 500, 1000\}$ W/m^2 are used to compute normalized ampacity distributions. These distributions are represented in Fig. 6 with blue colour, while their average is represented with red colour. The spread of normalized ampacity PDFs is relatively low for all sub-spaces, which means that the ambient temperature and the solar irradiance have relatively low impact on the normalized ampacity PDF. Therefore, the average of the corresponding distributions will be used as a representative PDF of a given sub-space of weather variables.

Next, we examine the impact of conductor type and emissivity on the ampacity uncertainty. We compare the ampacity distribution for the two most commonly used conductors in the Slovenian network: 243-AL1/39 and 490-AL1/64, and for three values of the emissivity: 0.2, 0.5 and 0.9. Fig. 7 shows the normalized ampacity distributions for both conductor types and all emissivity values when varying a single weather parameter at a time. In the first row, distributions are shown at ambient temperatures of 0 °C, 15 °C, and 30 °C; in the second row, for solar irradiance of 100 W/m^2, 500 W/m^2, and 1000 W/m^2; and in the last row, for wind angles of 0°, 45°, and 90°. In all calculations, the wind speed is 5 m/s. The results demonstrate that, for the given ranges
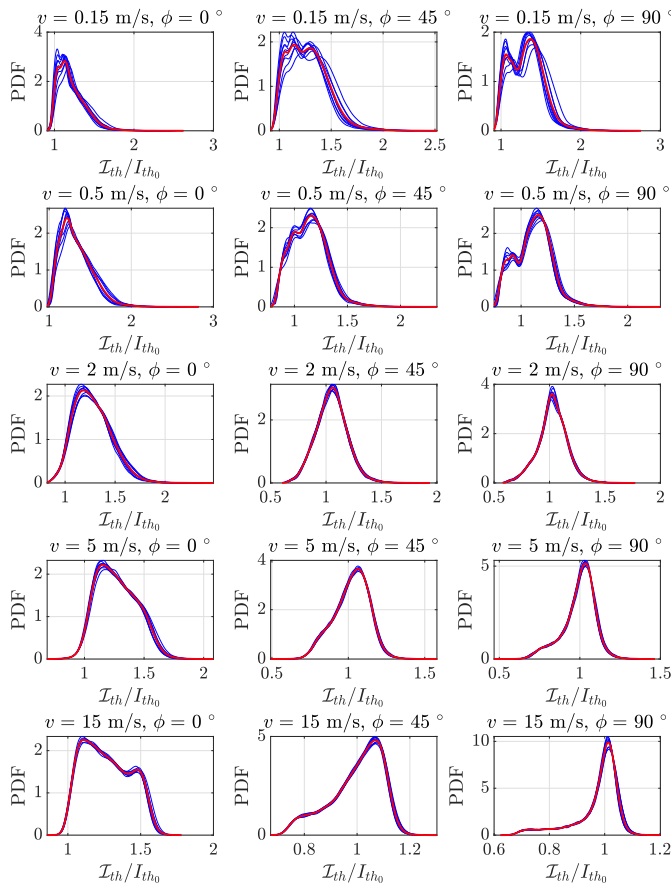
Fig. 6. Normalized ampacity distributions for different combinations of weather parameters. All plots are for conductor type 243-AL1/39 with emissivity of 0.9.

Fig. 7. Normalized ampacity distributions for two conductor types and three values of emissivity: 0.2, 0.5 and 0.9, and for different values of predicted weather parameters: air temperature (first row), solar irradiance (second row), and wind direction (third row). In all calculations, the wind speed is 5 m/s. In each graph, the highest peak is for emissivity of 0.9, the middle for emissivity of 0.5, and the lowest for emissivity of 0.2.

of weather parameters, the distributions are approximately the same for both conductor types. This was also confirmed by the Kolmogorov-Smirnov test for all the cases in Fig. 7. While we observe no major differences in the shape of the ampacity distributions, they however have different peaks due to different emissivity. The higher the peak, the higher is the emissivity of the conductor, as it allows higher ampacity.

We also examine the normalized ampacity distribution when the predicted wind speed varies (Fig. 8). We observe that for wind speeds of 5 m/s and 15 m/s, similarly to other before-mentioned weather parameters, the distributions are still practically the same (in shape) for both conductor types. This statement is again confirmed by Kolmogorov-Smirnov tests. We again observe small differences in the peaks due to different emissivities. However, the ampacity distributions for wind speeds of around 2 m/s and lower are visibly different in shape and peak height. Nevertheless, the Kolmogorov-Smirnov test again does not reject the hypothesis of equal distributions for different conductor types.

Besides the most commonly used conductors for the transmission lines, 243-AL1/39 and 490-AL1/64, we have also examined the ampacity distribution for other conductors used by the TSO: 243-ZTAL/39-HACIN, 149-AL1/24, 149-AL1/24 HACIN, and Cu80. Fig. 9 shows the normalized ampacity distributions for all listed conductors for different wind speeds,
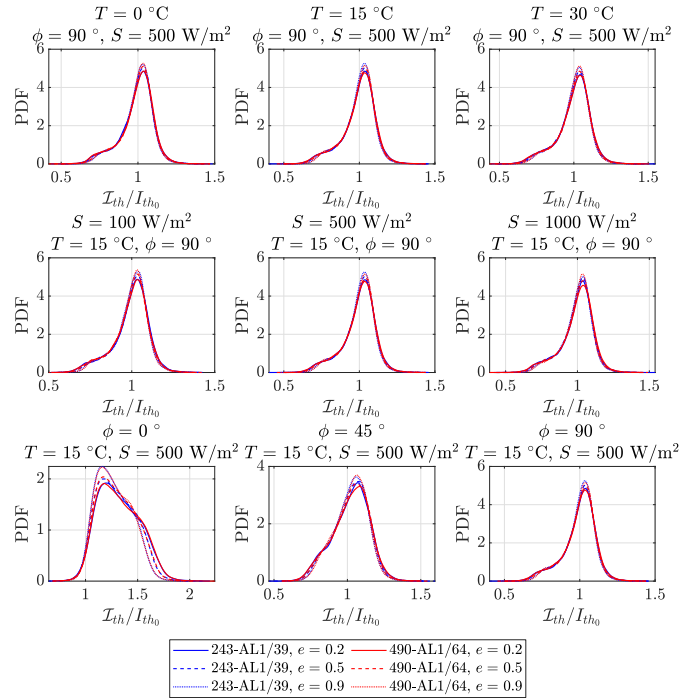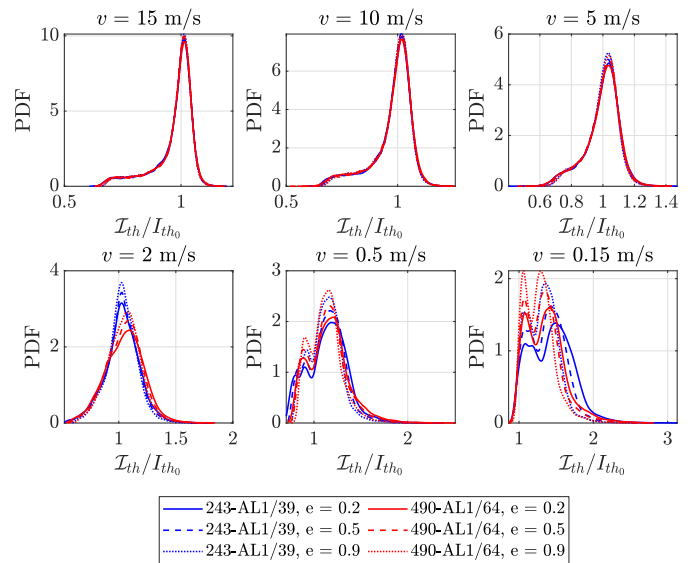

Fig. 8. Normalized ampacity distributions for two conductor types and three values of emissivity: 0.2, 0.5 and 0.9, and for different values of predicted wind speed. The values for the other parameters are: ambient temperature 15 °C, solar irradiance 500 W/m², and wind direction 90°.
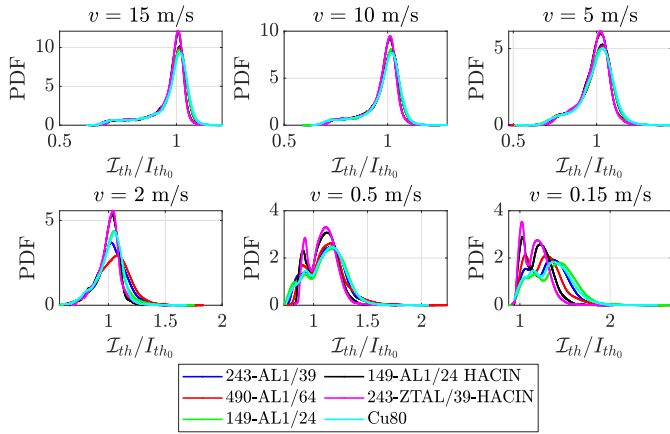
Fig. 9. Normalized ampacity distributions for all conductor types used by the TSO for different values of predicted wind speed. The values for the other parameters are: ambient temperature 15 °C, solar irradiance 500 W/m², wind direction 90°, and emissivity 0.9.

Fig. 10. Schematic representation of the operative DTR uncertainty estimation.

and for constant emissivity of 0.9 and wind direction of 90°. We can conclude that in the regimes of wind speed below 2 m/s, we can expect for the ampacity distributions to differ with conductor type and emissivity.

V. Implementation of operative DTR uncertainty assessment module

A schematic sketch of the operative DTR uncertainty assessment environment is shown in the Fig. 10. The pre-computed part - preparation of the ampacity distribution database - is on the right. Because the calculation of the ampacity probability distribution for a single combination of weather conditions and conduction properties would be computationally too demanding to be performed in real-time, the probability distributions are rather pre-computed for various combinations of input data and stored in a database. Based on the results of the pre-analysis, we have identified that the time horizon of the forecast, the wind speed and direction (from the weather parameters), and the conductor type and emissivity (from the material properties of the conductor), influence the normalized probability distribution of the ampacity the most. In accordance with those findings, therefore, in the space of weather and material variables, only a finite but large enough number of ampacity distributions are calculated for a finite number of their combinations. There is a total of 972 combinations stored in the database, which are made for: 3 values of forecast horizon (nowcast, short- and medium-term forecast), 6 wind speeds $v \in \{0.15; 0.5; 2; 5; 15\}$ m/s, 3 relative wind directions $\phi \in \{0, 45, 90\}°$, 6 conductor types, and 3 conductor emissivities $\epsilon \in \{0.2, 0.5, 0.9\}$.

The database is stored in a custom-made binary form, optimized for reading speed and minimal size. It is also accompanied by a set of Python tools for editing and viewing the database files. These tools are used when the database is generated by MC simulations, and can also be used to generate a new database from a new MC run on another set of weather data. It is important to note that it would take weeks for the database to be generated on a single computer.
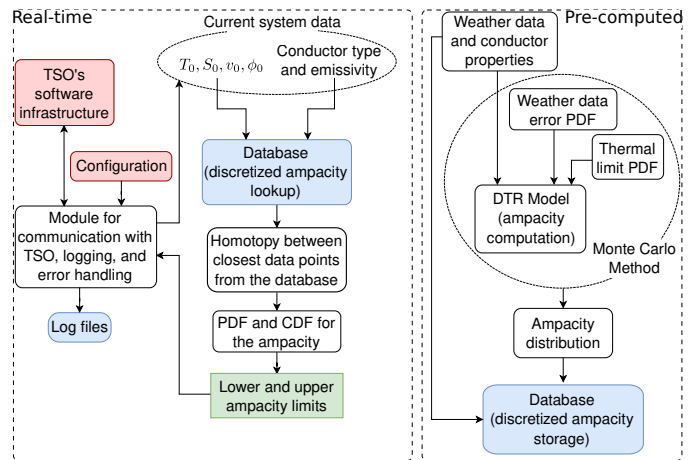
However, the MC approach is highly scalable on parallel computer architectures, so a computer cluster is best used to reduce the execution time. A new database has to be generated only when the input data changes significantly, e.g. when a new line is integrated into the system or after an additional year of weather data is available.

The left part of Fig. 10 shows how the real-time calculations are performed. The module implemented in C++ is compiled into a Linux shared library and is executed periodically to compute ampacity I_{th} with uncertainty from the supplied weather conditions, forecast horizon, conductor properties, the nominal ampacity I_{th_0} computed with DTR for the given weather conditions, and the desired confidence level. Ampacity CDFs for the data points nearest to the input of the algorithm are looked up from the database and transformed into the resulting ampacity CDF for the input using homotopy - a smooth transition from one distribution to another. Then the result is normalized with I_{th_0}. It should be noted that all the CDFs in the database and the resulting CDF from the procedure above are in a discrete form. A continuous form of CDF^{-1} is taken as the linearly interpolated inverse of the CDF, which is then finally used to calculate the confidence interval of the resulting ampacity as described in Section III.

We will demonstrate the homotopic rectilinear routing of the probability distributions for one weather variable. Note that in real use, the interpolation is multidimensional, as the weather variable space is. Let us assume that for some values of the temperature, the solar irradiance, the wind angle, and the conductor emissivity, we know the normalized ampacity distribution for wind speeds of 5 m/s and 15 m/s. If we need to obtain the ampacity distribution for a value of wind speed between 5 m/s and 15 m/s, we use homotopy between the probability distribution of the two nearest neighbors, i.e. the distributions at 5 m/s and 15 m/s. This is demonstrated in Fig. 11, where the red curve represents the distribution for wind speed of 15 m/s, and the blue curve represents the distribution for wind speed of 5 m/s, while the green curve is the result of homotopic rectilinear routing for two wind speed values between 5 m/s and 15 m/s.

This article has been accepted for publication in a future issue of this journal, but has not been fully edited. Content may change prior to final publication. Citation information: DOI 10.1109/TPWRS.2022.3144740, IEEE Transactions on Power Systems
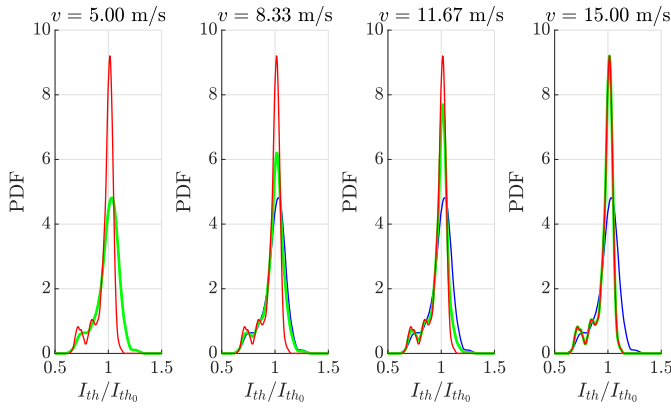
7

Fig. 11. Homotopic rectilinear routing from a normalized thermal flow distribution at wind speed of 5 m/s (blue curve) to a thermal flow distribution at wind speed of 15 m/s (red curve). The green curve is their linear combination or the result of homotopic rectilinear routing.
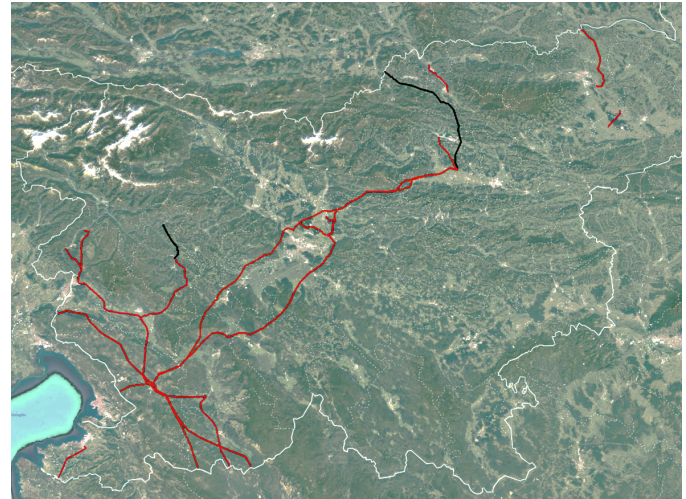

Fig. 12. An overview of the considered transmission system. The two lines investigated in this paper are plotted in black, while the others in red.
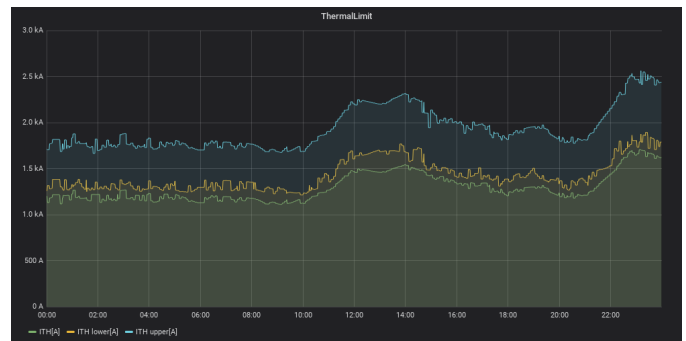

Fig. 13. Example plot from the module for DTR uncertainty assessment presenting the calculated ampacity with a given lower and upper limit for the Obersielach-Podlog transmission line on 12 July, 2020.

The execution time of the real-time module is dominated by the database lookup time. It is measured in tens to hundreds of milliseconds for a single system data point, which is currently efficient enough for the TSO. Lookups of multiple system data points, for example, for multiple lines or multiple time horizons, could be performed in parallel though, if required with future expansion of the TSO's system.

The underlying DTR software (DiTeR) at the TSO can run in two modes: as standalone software and as an embedded system within the SUMO framework – TSO's heterogeneous collection of subsystems from different vendors developed to increase safety and security, as well as the capacity of the existing transmission network [25]. For efficient integration into the SUMO framework, the developed DTR uncertainty assessment module uses the same API as the main DTR module and it is triggered after each DTR calculation. The results are communicated to the TSO's software infrastructure by a SOAP-based protocol. The main computational load is represented by the real-time calculations, which are triggered once every minute, and forecast calculations, which are repeated every 5 minutes, for all spans. Currently, the considered transmission system consists of 29 power lines with more than 2000 spans (Fig. 12).

The module for DTR uncertainty assessment was successfully incorporated into the Slovenian TSO's operational environment. An example of a result given by the module is given in Fig. 13. In the plot, the ampacity calculated by the current DTR model is presented with green line, while the lower and the upper limit of the ampacity, calculated by the new uncertainty assessment module, are presented with a yellow and blue line, respectively. In this example, we observe a situation when both the lower and the upper limit of the ampacity are greater than the nominal ampacity calculated with DTR. In scenarios with extremely low forecasted wind speeds, as in this case, the MC method certainly always samples more favorable cooling conditions, as the wind speed can only be positive. In an extreme case, the nominal ampacity computed on zero predicted wind speed is also the minimal ampacity, so all MC trials will give higher ampacity. Furthermore, on

Fig. 1, we can also observe that the wind speed forecast error is centered around 1 m/s, i.e. in the data we used, the measured wind speed is in average higher than the forecasted. Therefore, it is expected that in low wind regimes, the nominal ampacity will be in the lower part (less than 1) of the normalized ampacity PDF. In another words, it is expected that the actual ampacity in low or no wind prediction will be higher than the predicted one, as the low wind prediction stands for the worst case scenario.

As another example of using the implemented module, in Fig. 14 we present the statistics of the dynamic ampacity, taking into account its uncertainty, with respect to the static ampacity (645 A for the 243-AL1/39 conductor) and the measured load. An interesting conclusion from Fig. 14 is that, when taking into account realistic weather data, even the conservative static limit can be too high. We observed that, for the confidence level of 99%, the lower limit of the thermal current is lower than the static current for 5.21% of the time. Nevertheless, as expected, most of the time the dynamic ampacity is well above the static limit, and the actual load is always below the predicted ampacity.
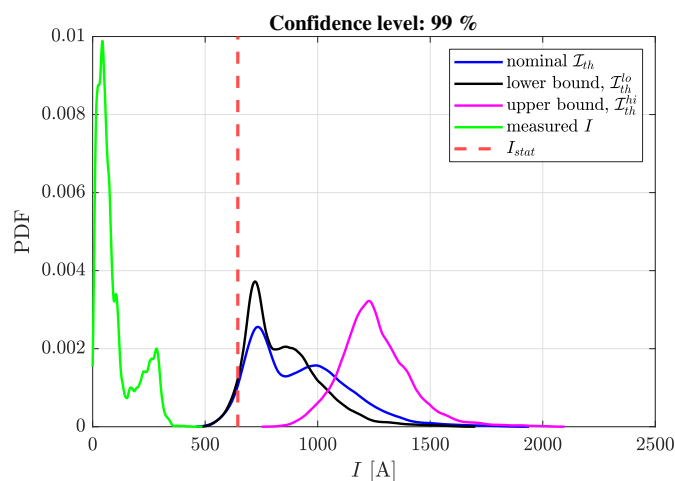
This article has been accepted for publication in a future issue of this journal, but has not been fully edited. Content may change prior to final publication. Citation information: DOI 10.1109/TPWRS.2022.3144740, IEEE Transactions on Power Systems

8

Fig. 14. Comparison of static, dynamic and measured current distributions for the Bevkov vrh location.

VI. Conclusions

In this paper, we presented a solution for estimating the uncertainty of the ampacity as a result of the DTR. First, we examined the weather forecast and measurement data, together with on-site measurements of conductor skin temperature, on two locations in Slovenia: Podlog and Bevkov vrh. We analyzed the dependence of the weather forecast error from the forecast horizon: nowcast, short-term forecast and medium-term forecast, with conclusion that there is no significant difference in quality between short-term and medium-term wind forecast. With the help of conductor surface temperature measurements, weather data measurements and predicted weather data, we estimated also the error of the DTR itself, with a clear conclusion that the majority of the ampacity forecast uncertainty originates from the weather forecast uncertainty. Furthermore, we demonstrated that the influence of the ambient temperature and the solar irradiance forecast error on the normalized ampacity distribution is much less important than the influence of the wind velocity forecast error. We also investigated the influence of different conductor types and their emissivity and have concluded that they are not negligible either.

Following the results of the data analyses, we designed and implemented a complete operational solution for estimating the DTR uncertainty. Using the Monte Carlo method, we randomly sampled the fitted-to-location error distributions of the input weather conditions and used the DTR model to calculate the ampacity distribution. In accordance with the findings, in the space of weather and material variables (two weather parameters and two material properties that significantly influence the normalized ampacity probability distribution), we calculated only a finite number of ampacity distributions for a finite number of input combinations and used homotopic rectilinear routing for computing intermediate values. When compared to previous related studies, this type of solution procedure for estimating the DTR uncertainty is presented for the first time in this paper. The developed solution was implemented as a stand-alone module and integrated into the

environment of the operator of the Slovenian electric power transmission network – ELES, where it is in operational use since August 2020.

The main limitation of this work is that the final result greatly depends on the available measured data. Nevertheless, the TSOs have great interest in installing new weather stations along the lines, and with steadily increasing the amount of available on-site weather data, the system will provide more reliable predictions, as it is designed to periodically update the distributions as more data becomes available. Future work will be focused on including ensemble weather predictions that inherently provide uncertainty for each specific weather parameter, which could be used on locations where measurements are not available.

References

[1] J. W. Bialek, "Why has it happened again? comparison between the ucte blackout in 2006 and the blackouts of 2003," in *2007 IEEE Lausanne Power Tech*. IEEE, 2007, pp. 51–56.

[2] A. Berizzi, "The italian 2003 blackout," in *IEEE Power Engineering Society General Meeting, 2004*. IEEE, 2004, pp. 1673–1679.

[3] *Guide for Thermal Rating Calculations of Overhead Lines*, CIGRE, 2014.

[4] M. Mahmoudian Esfahani and G. R. Yousefi, "Real Time Congestion Management in Power Systems Considering Quasi-Dynamic Thermal Rating and Congestion Clearing Time," *IEEE Transactions on Industrial Informatics*, vol. 12, no. 2, pp. 745–754, 2016.

[5] M. Dabbaghjamanesh, A. Kavousi-Fard, and S. Mehraeen, "Effective Scheduling of Reconfigurable Microgrids With Dynamic Thermal Line Rating," *IEEE Transactions on Industrial Electronics*, vol. 66, no. 2, pp. 1552–1564, 2019.

[6] M. Dabbaghjamanesh, A. Kavousi-Fard, S. Mehraeen, J. Zhang, and Z. Y. Dong, "Sensitivity Analysis of Renewable Energy Integration on Stochastic Energy Management of Automated Reconfigurable Hybrid AC–DC Microgrid Considering DLR Security Constraint," *IEEE Transactions on Industrial Informatics*, vol. 16, no. 1, pp. 120–131, 2020.

[7] G. Kosec, M. Maksić, and V. Djurica, "Dynamic thermal rating of power lines–model and measurements in rainy conditions," *International Journal of Electrical Power & Energy Systems*, vol. 91, pp. 222–229, 2017.

[8] P. Pytlak, P. Musilek, E. Lozowski, and J. Toth, "Modelling precipitation cooling of overhead conductors," *Electric Power Systems Research*, vol. 81, no. 12, pp. 2147–2154, 2011.

[9] S. Karimi, P. Musilek, and A. M. Knight, "Dynamic thermal rating of transmission lines: A review," *Renewable and Sustainable Energy Reviews*, vol. 91, pp. 600–612, 2018.

[10] M. Maksić, V. Djurica, A. Souvent, J. Slak, M. Depolli, and G. Kosec, "Cooling of overhead power lines due to the natural convection," *International Journal of Electrical Power & Energy Systems*, vol. 113, pp. 333–343, 2019.

[11] "IEEE Standard for Calculating the Current-Temperature Relationship of Bare Overhead Conductors," Dec. 2013.

[12] 2016. [Online]. Available: http://hdl.handle.net/2268/178855

[13] F. G. Erdinç, O. Erdinç, R. Yumurtacı, and J. P. Catalão, "A comprehensive overview of dynamic line rating combined with other flexibility options from an operational point of view," *Energies*, vol. 13, no. 24, p. 6563, 2020.

[14] D. A. Douglass, J. Gentle, H.-M. Nguyen, W. Chisholm, C. Xu, T. Goodwin, H. Chen, S. Nuthalapati, N. Hurst, I. Grant *et al.*, "A review of dynamic thermal line rating methods with forecasting," *IEEE Transactions on Power Delivery*, vol. 34, no. 6, pp. 2100–2109, 2019.

[15] J. L. Aznarte and N. Siebert, "Dynamic Line Rating Using Numerical Weather Predictions and Machine Learning: A Case Study," *IEEE Transactions on Power Delivery*, vol. 32, no. 1, pp. 335–343, 2017.

[16] F. Fan, K. Bell, and D. Infield, "Probabilistic Real-Time Thermal Rating Forecasting for Overhead Lines by Conditionally Heteroscedastic Auto-Regressive Models," *IEEE Transactions on Power Delivery*, vol. 32, no. 4, pp. 1881–1890, 2017.

[17] J. Zhan, C. Y. Chung, and E. Demeter, "Time Series Modeling for Dynamic Thermal Rating of Overhead Lines," *IEEE Transactions on Power Systems*, vol. 32, no. 3, pp. 2172–2182, 2017.

This article has been accepted for publication in a future issue of this journal, but has not been fully edited. Content may change prior to final publication. Citation information: DOI 10.1109/TPWRS.2022.3144740, IEEE Transactions on Power Systems

9

[18] A. Michiorri and P. C. Taylor, "Forecasting real-time ratings for electricity distribution networks using weather forecast data," in *Proceedings of the 20th International Conference and Exhibition on Electricity Distribution (CIRED)*, 2009.

[19] T. Ringelband, P. Schäfer, and A. Moser, "Probabilistic ampacity forecasting for overhead lines using weather forecast ensembles," *Electrical Engineering*, vol. 95, no. 2, pp. 99–107, 2013.

[20] D. Poli, P. Pelacchi, G. Lutzemberger, T. B. Scirocco, F. Bassi, and G. Bruno, "The possible impact of weather uncertainty on the dynamic thermal rating of transmission power lines: A monte carlo error-based approach," *Electric Power Systems Research*, vol. 170, pp. 338–347, 2019.

[21] G. Fishman, *Monte Carlo: Concepts, Algorithms and Applications*. New York: Springer-Verlag, 1996.

[22] E. Siwy, "Risk Analysis in Dynamic Thermal Overhead Line Rating," in *Proceedings of the International Conference on Probabilistic Methods Applied to Power Systems*, 2006.

[23] S. Karimi, A. M. Knight, P. Musilek, and J. Heckenbergerova, "A probabilistic estimation for dynamic thermal rating of transmission lines," in *Proceedings of the IEEE 16th International Conference on Environment and Electrical Engineering (EEEIC)*, 2016.

[24] Y. Wang, W. Tao, Z. Yan, and R. Wei, "Uncertainty analysis of dynamic thermal rating based on environmental parameter estimation," *EURASIP Journal on Wireless Communications and Networking*, 2018, article No. 167.

[25] G. Lakota, J. Kosmač, J. Kostevc, A. Souvent, and T. Fatur, "Real-time and short-term forecast assessment of power grid operating Limits-SUMO," in *Actual trends in development of Power System Relay Protection and Automation*, 2015.

Janko Kosmač studied at the University of Ljubljana, Slovenia, where he received his BSc (1990), MSc (1993) and PhD (1996) degrees. In 1996, he has been employed at the Elektroinštitut Milan Vidmar (EIMV), where he was leading the development of the Slovenian lightning localization system. In 2007, he was promoted to the head of the electric power system control and operation department at EIMV. He joined ELES, the Slovenian transmission system operator, in 2013. He is head of process system department and project manager of the dynamic thermal rating project at ELES.

Gregor Kosec (M'19) graduated at University of Ljubljana, Faculty of Mathematics and Physics in 2006 and obtained PhD in 2011 at the University of Nova Gorica. In 2011 he became a member of Parallel and Distributed Systems Laboratory at Jožef Stefan Institute. In 2020 he became head of the Parallel and Distributed Systems Laboratory. His main research interest covers computational modelling, meshless methods, and generic programming.

Aleksandra Rashkovska (M'14) received B.Sc. degree in Electrical Engineering from the University Ss. Cyril and Methodius, Skopje, Macedonia, in 2006, and Ph.D. degree in Computer Science from the Jožef Stefan International Postgraduate School, Ljubljana, Slovenia, in 2013. She is currently a Research Fellow at the Department of Communication Systems, Jožef Stefan Institute, Ljubljana, Slovenia. Her research interest includes advanced bio-signal analysis, computer simulations in biomedicine, biomedical applications of data mining and control theory, and data mining in sensor networks.

Mitja Jančič received the B.S. in physics continued to M.Sc. in mechanical engineering, both at the University of Ljubljana in Slovenia. He is currently in pursuit of a PhD at the Jožef Stefan international postgraduate school. He also holds the position of a research fellow at the Department of Communication Systems at the Jožef Stefan Institute in Ljubljana. His research interests include meshless methods, numerical procedures for solving PDE systems and generic programming algorithms.

Matjaž Depolli received a PhD in computer and information science from Jožef Stefan International Postgraduate School Ljubljana in 2010. He currently holds the position of research fellow at the Department of Communication Systems at the Jožef Stefan Institute in Ljubljana. His research interests include evolutionary computation, computer simulation of physical phenomena, parallel computing, and ECG analysis. He's been involved in the development of wireless body sensors, software for ECG analysis, cluster management software, and cloud services.